Commun. Comput. Phys.
doi: 10.4208/cicp.2009.08.135

Vol. **7**, No. 1, pp. 103-137
January 2010

Stable and Accurate Second-Order Formulation of the Shifted Wave Equation

Ken Mattsson[1,*] and Florencia Parisi[2]

[1] *Department of Information Technology, Uppsala University, P.O. Box 337, S-751 05 Uppsala, Sweden.*
[2] *FaMAF, Universidad Nacional de Córdoba, Medina Allende S/N Ciudad Universitaria, 5000 Córdoba, Argentina.*

Received 20 August 2008; Accepted (in revised version) 4 May 2009

Communicated by Chi-Wang Shu

Available online 16 July 2009

Abstract. High order finite difference approximations are derived for a one-dimensional model of the shifted wave equation written in second-order form. The domain is discretized using fully compatible summation by parts operators and the boundary conditions are imposed using a penalty method, leading to fully explicit time integration. This discretization yields a strictly stable and efficient scheme. The analysis is verified by numerical simulations in one-dimension. The present study is the first step towards a strictly stable simulation of the second-order formulation of Einstein's equations in three spatial dimensions.

AMS subject classifications: 35L05, 35L20, 65N06, 65N12, 83C05

Key words: High-order finite difference methods, wave equation, numerical stability, second derivatives, Einstein's equations.

1 Introduction

The present study is focused towards the numerical solution of Einstein's equations, which describe processes such as binary black holes and neutron star collisions. The outcome of this kind of simulations is considered to be crucial for the successful detection and interpretation of gravitational waves, expected to be measured by laser interferometers such as LIGO, GEO600, LISA and others. In turn, measurement of gravitational waves will constitute a strong, direct verification of Einstein's theory, and open a new window to the universe.

*Corresponding author. *Email addresses:* ken.mattsson@it.uu.se (K. Mattsson), fparisi@famaf.unc.edu.ar (F. Parisi)

In the harmonic description of general relativity, the principal part of Einstein's equations reduces to 10 curved space wave equations for the components of the space-time metric. Although these equations can be reduced to first-order symmetric hyperbolic form [7], this has the disadvantage of introducing auxiliary variables with their constraints and boundary conditions. The reduction to first-order form is also less attractive from a computational point of view considering the efficiency and accuracy [12,19]. The reasons for solving the equations on first-order form are most likely related to the maturity of CFD, which has evolved during the last 40 years. I.e., many of the stability issues for first-order hyperbolic problems have already been addressed.

Wave-propagation problems frequently require farfield boundaries to be positioned many wavelengths away from the disturbance source (for example binary black holes). To efficiently simulate these problems requires numerical techniques capable of accurately propagating disturbances (such as a gravitational wave) over long distances. It is well know that high-order finite difference methods (HOFDM) are ideally suited for problems of this type. (See the pioneering paper by Kreiss and Oliger [14]). Not all high-order spatial operators are applicable, however. For example, schemes that are G-K-S stable [9], while being convergent to the true solution as $\Delta x \to 0$, may experience non-physical solution growth in time [5], thereby limiting their efficiency for long-time simulations. Thus, it is imperative to use HOFDMs that do not allow growth in time; a property termed "strict stability" [8]. Deriving strictly stable, accurate and conservative HOFDM is a significant challenge that has received considerable past attention. (For example, see references [1,3,10,11,16,31–33,38]).

The energy method (see for example [8]) is a common technique to derive well-posedness for initial-boundary value problems. A very powerful way of obtaining provable strictly stable numerical approximations is to mimic the underlying continuous energy estimate. A well-proven HOFD methodology that ensures this is the summation-by-parts simultaneous approximation term (SBP-SAT) method. The SBP-SAT method simply combines finite difference operators that satisfy a summation-by-parts (SBP) formula [13], with physical boundary conditions implemented using either the Simultaneous Approximation Term (SAT) method [5], or the projection method [19,28,29]. Examples of the SBP-SAT approach can be found in references [6,15,17,18,20,22,24–27,34,35].

Deriving strictly stable numerical simulations of Einstein's equations on second-order form has proven to be a very difficult task [2,4,23,37], especially for HOFDMs. In the present study this situation is illustrated by the shifted wave equation in 1-D that captures most of the stability issues without introducing unnecessary complications. This 1-D problem was analyzed in [37] for a second-order accurate approximation.

For the Einstein's equations (and the shifted wave equation) written on second-order form, the regular energy estimate fails in the most interesting applications, which required the introduction of a modified energy estimate. The existing SBP-SAT method (here referred to as the *standard* SBP-SAT method) is based on the regular energy estimates, which means that the *standard* SBP-SAT method has to be modified in order to fit the mentioned modified energy estimate.

The goals of the present study are two-fold. The first one is to develop a systematic methodology, to guarantee, by construction, strict stability of the shifted wave equation using a narrow-stencil SBP-SAT method. The term *narrow-stencil* was introduced in [22] to define explicit finite difference schemes with a minimal stencil width. This task essentially requires the identification of the conditions that the SBP-SAT method must satisfy to guarantee strict stability and accuracy.

The second task is to demonstrate the new methodology. To this end, new high-order accurate finite difference SBP operators are derived suitably for the Einstein's equations written on second-order form.

The outline of the paper is the following: in Section 2 we derive the 1-D shifted wave equation from the Einstein's equations. The SBP property for the first- and second-derivative difference operators are discussed in Section 3, and we show an important relationship between them, referred to as *full compatibility*. (The term *compatible* was introduced in [22] as a necessary condition to prove stability for narrow-stencil approximations of the compressible Navier-Stokes equations. *full compatibility* is a more strict condition than *compatibility*). The first main result in the present study is the derivation of second-, fourth- and sixth-order accurate fully compatible SBP operators using the symbolic mathematics software Maple. In Section 4 we analyze the 1-D shifted wave equation using the energy method and an eigenvalue analysis. The second main result in this paper is to prove strict-stability using a modified SBP-SAT method combining: 1) the newly constructed fully compatible SBP operators, 2) SBP preserving artificial dissipation (first introduced in [21]), and 3) the newly derived modified SAT technique for implementing the physical boundary conditions. Finally, in Section 5, the accuracy and stability properties of the present method is verified by performing numerical simulations. Conclusions and future work are presented in Section 6.

2 The shifted wave equation

The present study is focused on the numerical stability issues concerning the shifted wave equation, a 1-D model of Einstein's equations. To make the connection between the shifted wave equation in 1-D and Einstein's equations we make a brief review of the harmonic description of General Relativity, in which the field equations can be written as a set of 10 curved wave equations for the space-time metric components. We will then use that review to argue that the geometric aspects, as well as the stability features of the problem can be fully captured by analyzing the properties of a shifted scalar wave equation in 1-D.

Harmonic coordinates $x^\mu \equiv (t,x^i) = (t,x,y,z)$ satisfy the wave equation in curved space given by

$$\Box_g x^\mu := \frac{1}{\sqrt{-g}} \partial_a \left(\sqrt{-g} g^{ab} \partial_b x^\mu \right) = 0, \tag{2.1}$$

where $g = det(g_{ab})$, g^{ab} is the inverse metric and $\Box_g$ denotes the wave operator in the

curved geometry defined by g_{ab}. In these coordinates Einstein's equations reduce to 10 quasilinear wave equations for the metric tensor of the form

$$\Box_g g^{ab} = S^{ab}, \tag{2.2}$$

where S^{ab} contains the non-linear terms that do not enter the principal part of the equation, and depends only on first derivatives of the metric. Now, the scalar wave equation given by

$$\Box_g u \equiv \frac{1}{\sqrt{-g}} \partial_a (\sqrt{-g} g^{ab} \partial_b u) = 0, \tag{2.3}$$

with u a scalar field, has the same principal part as (2.2) and it therefore represent a fundamental model that allows us to test the numerical algorithms derived in the present study, aiming to solve the full non-linear gravitational problem.

Consider, hence, as a first step, a simple 1-D problem (i.e, with one spacial coordinate) of (2.3). In this case $x^\mu = (t,x)$ and, by introducing the densitized inverse metric $\gamma^{ab} \equiv \sqrt{-g} g^{ab}$, the scalar wave equation reduces to

$$\partial_t(\gamma^{tt}\partial_t u) + \partial_t(\gamma^{tx}\partial_x u) + \partial_x(\gamma^{xt}\partial_t u) + \partial_x(\gamma^{xx}\partial_x u) = 0. \tag{2.4}$$

If we now express the metric γ^{ab} in the usual ADM variables (introduced by **A**rnowitt, **D**eser and **M**isner) by defining the lapse ($\mathcal{N}$) and shift (a) functions by means of a foliation of the space-time into spacial hypersurfaces Σ_t parametrized by a time function t, then our 1-D (2.4) takes the form of the following shifted wave equation

$$-\partial_{tt} u + \partial_t(a\partial_x u) + \partial_x(a\partial_t u) + \partial_x((b-a^2)\partial_x u) = 0. \tag{2.5}$$

Here b is a smooth coefficient (directly related to the lapse $\mathcal{N}$) assumed to satisfy $b>0$. In this expression we have taken for simplicity and without loss of generality $\gamma^{tt} = -1$ for the extra term that would otherwise appear in the equation is a lower order term. Hence, it depends only on the first time-derivative of γ^{tt}, and does not enter in the principal part (it can be absorbed into the tensor S^{ab}).

Remark 2.1. The coefficient $b-a^2$ ($\equiv \gamma^{xx}$ in general relativity, and $\equiv c$ in the present study) in (2.5) determines the character of the space-time foliation. For example, $b-a^2>0$ and $b>0$ means that the t-foliation is spacial and the space-time metric has lorentzian signature. There is an event horizon where $b=a^2$ while $b-a^2<0$ implies that the time flow vector (t^a) becomes spacial, which would correspond to a region inside the horizon of a black hole.

To summarize: When harmonic coordinates are introduced, Einstein's equations reduce to a set of curved wave equations whose principal part is identical to that in the simple model of the shifted wave equation

$$u_{tt} - (au_x)_t - (au_t)_x - ((b-a^2)u_x)_x = 0. \tag{2.6}$$

(We have, for compactness, changed the derivative notation to subindex.) As a consequence we will, from now on, refer to (2.6) as a 1-D model of Einstein's equations, with the assumption that b is positive. In the present study we will analyze the stability and accuracy properties of this model, with the intention to generalize it to the full 3-D problem in a coming study. We note that (2.6) can be written as

$$(\partial/\partial t-\lambda_1\partial/\partial x)(\partial/\partial t-\lambda_2\partial/\partial x)u=0, \tag{2.7}$$

indicating the characteristics. Here

$$\lambda_{1,2}=a\pm\sqrt{b} \quad , \quad -\lambda_1\lambda_2=b-a^2\equiv c. \tag{2.8}$$

The model (2.6) was analyzed in [37], using a narrow-stencil second-order non-SBP discretization. Furthermore, only the half-plane problem was analyzed for the case $c<0$ (corresponding to a region inside the event horizon) in that study, thus avoiding the problem of implementing physical boundary conditions. In the present study we want to extend the analysis in [37] to a higher-order narrow-stencil SBP-SAT method, including the implementation of the physical boundary conditions (especially for $c<0$).

3 Definitions

The following definitions are needed in Section 4, to derive and analyze the numerical approximations of the shifted wave equation. Let the inner product for real-valued functions $u,v\in L^2[0,1]$ be defined by

$$(u,v)=\int_0^1 uvwdx, \quad w(x)>0,$$

and let the corresponding norm be $\|u\|_w^2=(u,u)$. The domain $(0\le x\le 1)$ is discretized using $N+1$ equidistant grid points,

$$x_i=ih, \quad i=0,1,\cdots,N, \quad h=\frac{1}{N}.$$

The approximate solution at grid point x_i is denoted v_i, and the discrete solution vector is $v^T=[v_0,v_1,\cdots,v_N]$. Similarly, we define an inner product for discrete real-valued vector functions $u,v\in\mathbf{R^{N+1}}$ by

$$(u,v)_H=u^THv, \quad H=H^T>0,$$

with the corresponding norm $\|v\|_H^2=v^THv$. The following vectors will be frequently used:

$$e_0=[1,0,\cdots,0]^T, \quad e_N=[0,\cdots,0,1]^T. \tag{3.1}$$

3.1 Narrow-diagonal SBP operators

To define narrow-diagonal SBP operators, we present the following definition (first stated in [22]):

Definition 3.1. *An explicit pth-order accurate finite-difference scheme with minimal stencil width of a Cauchy problem is called a pth-order accurate narrow stencil.*

We say that a scheme is explicit if no linear system of equations need to be solved to compute the difference approximation. Spatial Padé discretizations [16] are often referred to as "compact schemes". The approximation of the derivative is obtained by solving a tri- or penta-diagonal system of linear equations at every time step. Hence, if written in explicit form, Padé discretizations lead to full-difference stencils, similar to spectral discretizations.

The following two Definitions are central to the present study (first stated in [22]),

Definition 3.2. *A difference operator $D_1 = H^{-1}Q$ approximating $\partial/\partial x$, using a pth-order accurate narrow stencil, is said to be a pth-order accurate narrow-diagonal first-derivative SBP operator, if H is diagonal and positive definite, and*

$$Q+Q^T = B = diag(-1,0\cdots,0,1).$$

For hyperbolic problems on second-order form, we need an SBP operator for the second-derivative. Consider the wave equation (excluding the boundary conditions)

$$u_{tt} = (cu_x)_x. \tag{3.2}$$

Multiplication of Eq. (3.2) by u_t and integration by parts (referred to as"the energy method") leads to

$$\frac{d}{dt}\left(\|u_t\|^2 + \|u_x\|_c^2\right) = 2cu_tu_x|_0^1. \tag{3.3}$$

Definition 3.3. *Let $D_2^{(c)} = H^{-1}(-M+CS)$ approximate $\partial/\partial x(c\partial/\partial x)$, where $c(x) > 0$ is a smooth function, using a pth-order accurate narrow stencil. $D_2^{(c)}$ is said to be a pth-order accurate narrow-diagonal second-derivative SBP operator, if H is diagonal and positive definite, M is symmetric and positive semi-definite, S approximates the first-derivative operator at the boundaries and $C = diag(-c_0,0,\cdots,0,c_N)$.*

(High-order accurate narrow-diagonal second-derivative SBP operators for constant coefficients $c(x) = 1$, denoted D_2, were constructed in [18].) An example of its use is the semi-discretization $v_{tt} = D_2^{(c)}v$ of Eq. (3.2). Multiplying by $v_t^T H$ and adding the transpose leads to

$$\frac{d}{dt}\left(\|v_t\|_H^2 + v^TMv\right) = 2(v_t)_N(CSv)_N - 2(v_t)_0(CSv)_0. \tag{3.4}$$

Estimate (3.4) is a discrete analog of Eq. (3.3). Notice that obtaining energy estimates for schemes utilizing both D_1 and $D_2^{(c)}$ requires that both are based on the same norm H.

Remark 3.1. The boundary closure for a *pth*-order accurate narrow-diagonal SBP operator is of order $p/2$ (see [18]). This means that the boundary closure for $(D_1)^2 \equiv D_1 D_1$ is of order $p/2-1$. Hence, for second-order hyperbolic systems the convergence for wide-stencil approximations (i.e., by replacing D_2 with $(D_1)^2$) drops to $(p/2+1)th$-order, while the narrow-stencil formulations are $(p/2+2)th$-order accurate (see [36] for more information on the accuracy of finite difference approximations).

Remark 3.2. An SBP operator is essentially a centered difference scheme with a specific boundary treatment. In the Appendix we present both finite difference stencils with and without a SBP closure for the fourth- and the sixth-order accurate cases. The finite difference stencils without a SBP closure will be referred to as non-SBP operators. The boundary closures of the sixth-order non-SBP operators are chosen to produce sixth-order accurate stencils (compared to the third-order accurate boundary closures for the SBP operators). The fourth-order non-SBP operator is presented in [31], where it is used to derive HOFDM for the compressible Navier-Stokes equations. (In the present study, the fourth-order accurate non-SBP operator will be used in a new environment, not originally intended for. We introduce it here merely to motivate the importance of the SBP property for numerical simulations of the shifted wave-equation).

There are two options for obtaining a narrow-stencil approximation of (3.2). The first option (as shown above) is to approximate $(cu_x)_x$ using a narrow-diagonal second-derivative SBP operator $D_2^{(c)}$, to exactly mimic the continuous estimate (3.3). (A second-order accurate narrow-diagonal second-derivative SBP operator $D_2^{(c)}$ is presented in the Appendix.) The drawback so far with this approach is that $D_2^{(c)}$ is limited to second-order accuracy. The second approach is to discretize the expanded form $c_x u_x + c u_{xx}$ (using the constant coefficient narrow-diagonal SBP operators), leading to

$$v_{tt} = \bar{C}_x D_1 v + \bar{C} D_2 v = H^{-1}(\bar{C}_x Q - \bar{C} M) v + H^{-1} C S v.$$

The diagonal matrices $\bar{C}$ and $\bar{C}_x$ have the values of c and c_x injected on the diagonal. A sufficient stability condition for this discretization is that the eigenvalues of $\bar{C}_x Q - \bar{C} M$ are non-positive and strictly real (assuming that the boundary conditions are implemented in a stable way, which will be the task of the coming section). For the constant coefficient case this condition is guaranteed since M by construction is symmetric and positive semi-definite. For the variable coefficient case, an eigenvalue analysis (not shown here) for various test-functions $c(x) > 0$ (and number of unknowns) indicates that the eigenvalues to $\bar{C}_x Q - \bar{C} M$ are non-positive and strictly real using the SBP operators presented in the Appendix.

Remark 3.3. Definitions 3.1-3.3 were first stated in [22]. To improve readability these definitions have been repeated in the present study. We now continue this section with completely new material.

The following definition is crucial to the present study:

Definition 3.4. *Let D_1 and D_2 be pth-order accurate narrow-diagonal first- and second-derivative SBP operators in the same norm H. If*

$$D_2 = H^{-1}(-D_1^T H D_1 - R^{(p)} + B D_1),$$

and the remainder $R^{(p)}$ is positive semi-definite, D_1 and D_2 are called fully compatible.

Employing the first-derivative SBP operator twice (leading to a wide stencil) yields $D_1 D_1 = H^{-1}(-D_1^T H D_1 + B D_1)$. Hence, for fully compatible *pth*-order accurate SBP operators, the following property holds:

$$D_2 = D_1 D_1 - H^{-1} R^{(p)},$$

where $R^{(p)}$ is symmetric and positive semi-definite.

The first main result in the present study is the derivation of fully compatible SBP operators for the second-, fourth- and sixth-order accurate cases using the symbolic mathematics software Maple. For a detailed study of how to construct the traditional first- and second-derivative SBP operator see [13] and [18] respectively. SBP operators sometimes (depending on the order of accuracy) have "free" parameters after the accuracy and SBP conditions have been enforced. Since the full compatibility relation introduce an extra (new) condition (defined in Definition 3.4) we need more "free" parameters (compared to the traditional SBP operators case). This is the reason why the newly constructed fully compatible SBP-operators incorporate more boundary points (two more at each boundary to be precise, except for the second-order case) compared to the traditional SBP operators derived in [13, 18]. The fully compatible SBP operators are presented in the Appendix.

For the Cauchy problem, i.e., disregarding the one-sided boundary closures of the SBP operators, the following relations for the remainders $R^{(p)}$ ($p = 2,4,6,8$) hold:

$$\begin{aligned}
-R^{(2)} &= -\frac{h^3}{4} D_4, \\
-R^{(4)} &= +\frac{h^5}{18} D_6 - \frac{h^7}{144} D_8, \\
-R^{(6)} &= -\frac{h^7}{80} D_8 + \frac{h^9}{600} D_{10} - \frac{h^{11}}{3600} D_{12}, \\
-R^{(8)} &= +\frac{h^9}{350} D_{10} - \frac{h^{11}}{2520} D_{12} + \frac{h^{13}}{14700} D_{14} - \frac{h^{15}}{78400} D_{16},
\end{aligned} \tag{3.5}$$

where $D_{2n} = (D_+ D_-)^n$ is an approximation of $\frac{d^{2n}}{dx^{2n}}$. For example,

$$\frac{1}{h^2}(D_+ D_- v)_j = (v_{j+1} - 2v_j + v_{j-1})$$

is the second-order accurate narrow second-derivative finite-difference approximation.

The action of a derivative of order n on a pure Fourier mode $e^{i\omega x}$, results in $(i\omega)^n e^{i\omega x}$. The second-derivative, for example, gives $-\omega^2 e^{i\omega x}$. Consider the same Fourier mode on a grid over $[-1,1]$ with grid spacing h. The Fourier mode defined on the grid is given by $\hat{u}^T=[e^{i\omega x_0},e^{i\omega x_1},\cdots,e^{i\omega x_N}]$. It is convenient to introduce a scaled wavenumber $k=\omega h$, where $k\in[0,\pi]$. The Fourier mode for the wavenumber $k=\pi$, is $\hat{u}^T=[1,-1,1,\cdots,-1]$ (the highest frequency that can exist on the grid). It can be shown that a centered, second-order accurate difference operator of order n, applied to a Fourier mode results in

$$D_n\hat{u}=\left(\frac{2i}{h}\right)^n\hat{u}\sin^n\left(\frac{k}{2}\right).$$

This shows that $-R^{(p)}$ constitutes only dissipative terms.

Definition 3.5. *Let $R^{(p)}$ be the remainder for the Cauchy problem, given by Eq. (3.5). Let $\tilde{R}^{(p)}$ be defined as the minimal stencil, such that $\tilde{R}^{(p)}\hat{u}\geq R^{(p)}\hat{u}$. Then we say that $\tilde{R}^{(p)}$ dominates $R^{(p)}$.*

For the Cauchy problem $\tilde{R}^{(p)}$ ($p=2,4,6,8$) is given by:

$$\tilde{R}^{(2)}=\frac{h^3}{4}D_4,\quad \tilde{R}^{(4)}=-\frac{h^5}{12}D_6,\quad \tilde{R}^{(6)}=\frac{17h^7}{720}D_8,\quad \tilde{R}^{(8)}=-\frac{2h^9}{315}D_{10}. \tag{3.6}$$

Definition 3.6. *Let $R^{(p)}$ be the remainder for the boundary-value problem. Let $\tilde{R}^{(p)}$ be defined as the minimal stencil, such that the eigenvalues of $(\tilde{R}^{(p)}-R^{(p)})$ are non-negative. Then we say that $\tilde{R}^{(p)}$ dominates $R^{(p)}$.*

For the boundary-value problem, an eigenvalue analysis results in

$$\tilde{R}^{(2)}=1.00\frac{h^3}{4}D_2^TD_2,\quad \tilde{R}^{(4)}=1.06\frac{h^5}{12}D_3^TD_3,\quad \tilde{R}^{(6)}=2.94\frac{17h^7}{720}D_4^TD_4, \tag{3.7}$$

where $(D_{2,3,4})v$ are consistent approximations of u_{xx},u_{xxx} and u_{xxxx}, respectively (see [21]).

The compatibility relation so far is defined only for the constant coefficient case. By employing the first-derivative SBP operator twice (resulting in a wide-stencil approximation), the semi-discretization of (3.2) is given by

$$v_{tt}=H^{-1}(-D_1^T\bar{C}HD_1+CD_1)v,$$

leading to an energy estimate that exactly mimics the continuous energy estimate (3.3). By using the split form and the fully compatible first- and second-derivative SBP operators the semi-discretization of (3.2) is given by

$$v_{tt}=H^{-1}(\bar{C}_xQ-\bar{C}M+CD_1)v.$$

The following definition is central to the present study:

Definition 3.7. *Let D_1 and D_2 be pth-order accurate fully compatible first- and second-derivative SBP operators. If*

$$\bar{C}_x Q - \bar{C} M = -D_1^T H \bar{C} D_1 - R_c^{(p)},$$

and the remainder $R_c^{(p)}$ is positive semi-definite for $c(x)>0$, D_1 and D_2 are called fully compatible for $c(x)>0$.

Remark 3.4. $D_1 = H^{-1}Q$ and $D_2 = H^{-1}(-M+CD_1)$ is defined in Definitions 3.2 and 3.3. (The boundary derivative operator CS in Definition 3.3 is equal to CD_1 if D_1 and D_2 are fully compatible.) The diagonal matrices $\bar{C}$ and $\bar{C}_x$ have the values of c and c_x injected on the diagonal. The newly constructed fully compatible SBP operators presented in the Appendix, have been found to be fully compatible for $c(x)>0$, for various test-functions $c(x)>0$.

Definition 3.8. *Let $R_c^{(p)}$ be the remainder for the boundary-value problem. Let $\tilde{R}_c^{(p)}$ be defined as the minimal stencil, such that the eigenvalues of $(\tilde{R}_c^{(p)} - R_c^{(p)})$ are non-negative. Then we say that $\tilde{R}_c^{(p)}$ dominates $R_c^{(p)}$.*

An eigenvalue analysis results in the following operators

$$\tilde{R}_c^{(2)} = h^3 D_2^T |\bar{C}| D_2, \quad \tilde{R}_c^{(4)} = \frac{h^5}{4} D_3^T |\bar{C}| D_3, \quad \tilde{R}_c^{(6)} = \frac{17h^7}{120} D_4^T |\bar{C}| D_4. \tag{3.8}$$

4 Analysis

The main motivation of the present study is to analyze and resolve the stability issues for narrow-stencil approximations of the shifted wave equation (2.6), for the case $c<0$. We will derive the necessary stability conditions using a modified SBP-SAT method, based on the fully compatible SBP operators constructed in the present study.

4.1 The constant coefficient 1-D problem

We begin studying the constant coefficient problem

$$u_{tt} - 2au_{xt} - cu_{xx} = 0, \tag{4.1}$$

(obtained by linearizing and freezing the coefficients in (2.6)), before we go on with the more interesting non-constant coefficient problem. Artificial boundaries are introduced at $x=0,1$. The energy method in combination with the signs of $\lambda_{1,2}$ are used to derive well-posed boundary conditions. The regular technique (see Section 3) of multiplying Eq. (4.1) by u_t and integrating by parts leads to

$$\frac{d}{dt} E_0 = 2u_t(au_t + cu_x)|_0^1, \tag{4.2}$$

where

$$E_0 = \left(\|u_t\|^2 + \|u_x\|_c^2 \right). \tag{4.3}$$

This is a valid energy for $c \geq 0$, but not for $c < 0$. To obtain an energy for $c < 0$, we multiply Eq. (4.1) by $u_t - a u_x$ and integrate by parts to obtain

$$\frac{d}{dt} E_1 = \left(\frac{\lambda_1}{2} (u_t - \lambda_2 u_x)^2 + \frac{\lambda_2}{2} (u_t - \lambda_1 u_x)^2 \right) |_0^1, \tag{4.4}$$

where

$$E_1 = \left(\|u_t - a u_x\|^2 + \|u_x\|_b^2 \right). \tag{4.5}$$

This is a valid energy for any c, provided $b \geq 0$. The main focus in the present study is to devise a stable and accurate narrow-stencil approximation to Eq. (4.1), including the boundary treatment.

To obtain a well-posed problem we close Eq. (4.1) with appropriate boundary conditions (depending on the sign of c). With no restriction we assume that $a > 0$ (if $a < 0$ the number of boundary conditions to be specified at each boundary is reversed). We have three different scenarios: $c > 0$, $c = 0$ and $c < 0$.

Case 1, $c > 0$

If $c > 0$ the direction of the characteristics (Eq. (2.7)) – shows that we need to specify one boundary condition at each boundary. The characteristic boundary conditions (CBC) are given by

$$\begin{aligned} L_0 u &= u_t - \lambda_1 u_x = g_0, \quad x = 0, \\ L_1 u &= u_t - \lambda_2 u_x = g_1, \quad x = 1. \end{aligned} \tag{4.6}$$

To simplify the analysis we assume that the boundary data is homogeneous ($g_0 = g_1 = 0$). The analysis also holds for inhomogeneous data, but introduces unnecessary notation. The energy method applied to Eq. (4.1) with the CBCs (4.6) leads to

$$\frac{d}{dt} E_0 = -2\sqrt{b} (u_{0t})^2 - 2\sqrt{b} (u_{1t})^2, \tag{4.7}$$

or

$$\frac{d}{dt} E_1 = -\frac{2\sqrt{b}}{\lambda_1} (u_{0t})^2 + \frac{2\sqrt{b}}{\lambda_2} (u_{1t})^2. \tag{4.8}$$

Here the following notation is used: $u_0 \equiv u(x=0)$ and $u_1 \equiv u(x=1)$.

A semi-discretization of (4.1) using narrow-diagonal SBP operators D_1, D_2, and the SAT method to impose the CBCs (4.6), can be written as

$$v_{tt} - 2aD_1 v_t - cD_2 v = SAT_0 + SAT_1, \tag{4.9}$$

where the penalty terms above are given by $SAT_0 = \tau_0 H^{-1} e_0 (L_0^T v - g_0)$ and $SAT_1 = \tau_1 H^{-1} e_N (L_1^T v - g_1)$ with e_0 and e_N given by Eq. (3.1). The discrete versions of the CBCs (4.6) are

$$\begin{aligned} L_0^T v &= v_t - \lambda_1 (Sv)_0 = g_0, \\ L_1^T v &= v_t - \lambda_2 (Sv)_N = g_1. \end{aligned} \tag{4.10}$$

Lemma 4.1. *The scheme* (4.9) *with homogeneous data is stable for* $c > 0$*, if* $D_{1,2}$ *are narrow-diagonal SBP operators,* $\tau_0 = \lambda_2$ *and* $\tau_1 = -\lambda_1$.

Proof. Let $g_0 = g_1 = 0$. Multiplying Eq. (4.9) by $v_t^T H$ from the left and adding the transpose leads to

$$\begin{aligned} \frac{d}{dt}(\|v_t\|_H^2 + c v^T M v) = & 2(v_{0t})^2(-a+\tau_0) + 2(v_{Nt})^2(a+\tau_1) \\ & - 2(v_0)_t (Sv)_0 (c + \tau_0 \lambda_1) + 2(v_N)_t (Sv)_N (c - \tau_1 \lambda_2), \end{aligned}$$

assuming that M is symmetric. To obtain an energy estimate requires that M is positive semi-definite, $\tau_0 = -c/\lambda_1 \equiv \lambda_2$ and $\tau_1 = c/\lambda_2 \equiv -\lambda_1$. This leads to

$$\frac{d}{dt}(\|v_t\|_H^2 + c v^T M v) = -2\sqrt{b}(v_{0t})^2 - 2\sqrt{b}(v_{Nt})^2,$$

which exactly mimics the continuous estimate (4.7). By assumption, D_2 is a narrow-stencil SBP operator, meaning that M is both symmetric and positive semi-definite. □

For the present case $c > 0$ the standard SBP-SAT method leads to an energy estimate that exactly mimics the continuous energy estimate, thus proving strict-stability. It is presented here for completeness. It is important to remember that the SBP-SAT method consists of two parts. The first part is the SBP property of the finite difference stencils $D_{1,2}$. (An SBP operator is essentially a centered difference scheme with a specific boundary treatment.) In Fig. 1 we display the eigenvalues to Eq. (4.9) (with $a = 1$, $b = 2$ and $N = 51$) using both SBP and non-SBP operators $D_{1,2}$ for the sixth-order case. The treatment of the physical boundary conditions using the SAT technique is kept identical for the SBP and non-SBP cases, to isolate the effect of the SBP property. All operators are presented in Appendix.

Lemma 4.1 shows that the energy (and thus the solution) is bounded when employing the SBP-SAT method, implying that the eigenvalues to (4.9) must be non-positive. This is also verified in Fig. 1, where the largest real part is $3.40 \cdot 10^{-14}$ for the SBP-SAT method. The corresponding result when using the non-SBP operators results in eigenvalues with positive real part (the largest real part is 60.44), thus resulting in an unstable scheme.

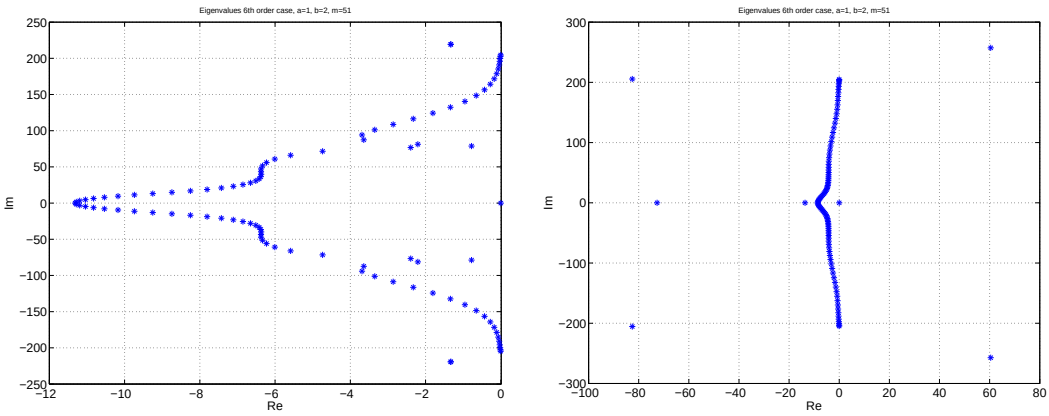

Figure 1: The eigenvalues to Eq. (4.9) for the sixth-order case, comparing a SBP closure (left) and a non-SBP closure (right). $b=2, a=1, N=51$.

Case 2, $c=0$

If $c=0$, Eq. (4.1) reduces to a hyperbolic first-order problem. In this case $\lambda_2=0$ and $\lambda_1>0$ (for $a>0$), meaning that we need to specify only one boundary condition $u_t=g$, at $x=0$. The energy method applied to Eq. (4.1) leads to

$$\frac{d}{dt}\|u_t\|^2=2a(g^2-(v_{0t})^2). \tag{4.11}$$

A semi-discretization of (4.1) is given by

$$v_{tt}-2aD_1v_t=-2a\tau H^{-1}e_0((v_N)_t-g), \tag{4.12}$$

and, by applying the energy method to this expression, we obtain

$$\frac{d}{dt}\|v_t\|_H^2=2a\left(\frac{\tau^2}{2\tau-1}g^2-(v_{0t})^2-(2\tau-1)\left((v_N)_t-\frac{\tau}{2\tau-1}g\right)^2\right).$$

An energy estimate exists for $\tau>1/2$. The choice $\tau=1$ yields

$$\frac{d}{dt}\|v\|_H^2=2a\Big(g^2-(v_0)^2-((v_N)_t-g)^2\Big),$$

which is a discrete analog of the integration by parts formula Eq. (4.11) in the continuous case, where the extra term $((v_N)_t-g)^2$ introduces a small additional damping.

Case 1, $c<0$

If $c<0$, an energy estimate can be derived considering the energy E_1 shown in Eq. (4.5), which is obtained by multiplying Eq. (4.1) by u_t-au_x and integrating by parts. For the

semi-discrete approximation, this complicates the imposition of boundary conditions using SAT. We begin studying this case with the exclusive usage of first-derivative SBP operators (here referred to as the *wide-stencil* approximation), to show that the stability problems are not restricted to the narrow-stencil approximation (although the narrow-stencil approximation introduces some additional complications, shown later in this section).

With $c<0$ we need to specify two boundary conditions at $x=1$. No boundary conditions should be given at $x=0$ (with $a<0$ it is the other way around, i.e., two boundary conditions at $x=0$ are needed). Well-posed boundary conditions are given by

$$\begin{aligned} L_{11}u &= u_t = g_{11}, \quad x=1, \\ L_{12}u &= u_x = g_{12}, \quad x=1, \end{aligned} \tag{4.13}$$

or, alternatively, we can impose CBCs of the form

$$\begin{aligned} L_{13}u &= u_t - \lambda_1 u_x = g_{13}, \quad x=1, \\ L_{14}u &= u_t - \lambda_2 u_x = g_{14}, \quad x=1. \end{aligned} \tag{4.14}$$

To simplify the analysis we assume homogeneous boundary data (once more, the analysis holds for inhomogeneous data, but introduces unnecessary notation.) The energy method applied to Eq. (4.1) with the boundary conditions (4.13) leads to

$$\frac{d}{dt}E_1 = -\left(\frac{\lambda_1}{2}(u_t-\lambda_2 u_x)^2+\frac{\lambda_2}{2}(u_t-\lambda_1 u_x)^2\right)\Big|_{x=0}. \tag{4.15}$$

The wide-stencil approximation of (4.1) employing the SBP-SAT method to impose the boundary conditions (4.13) can be written as

$$v_{tt}-2aD_1v_t-cD_1D_1v=SAT_2. \tag{4.16}$$

The penalty term is given by

$$SAT_2=\tau_{11}H^{-1}e_N(L_{11}^Tv-g_{11})+\tau_{12}H^{-1}e_N(L_{12}^Tv-g_{12})$$

where the discrete approximations of the boundary conditions (4.13) are given by

$$\begin{aligned} L_{11}^Tv &= (v_N)_t = g_{11}, \\ L_{12}^Tv &= (D_1v)_N = g_{12}. \end{aligned} \tag{4.17}$$

To simplify the analysis we assume that the boundary data is homogeneous. (The analysis holds for inhomogeneous data, but introduces unnecessary notation.) Multiplying Eq. (4.16) by $v_t^TH-av^TQ^T$ from the left and adding the transpose leads to

$$\frac{d}{dt}(E_1)_H = x_N^T\tilde{R}_Nx_N-x_0^TR_0x_0,$$

where we have introduced the discrete energy

$$(E_1)_H = (\|v_t - aD_1 v\|_H^2 + b\|D_1 v\|_H^2). \tag{4.18}$$

Here $x_{0,N}^T = [(v_{0,N})_t, (D_1 v)_{0,N}]$ and

$$\tilde{R}_N = \begin{bmatrix} a+2\tau_{11} & c-a\tau_{11}+\tau_{12} \\ c-a\tau_{11}+\tau_{12} & -ac-2a\tau_{12} \end{bmatrix}, \quad R_0 = \begin{bmatrix} a & c \\ c & -ac \end{bmatrix}. \tag{4.19}$$

Since R_0 is positive definite, stability follows if $\tilde{R}_N$ can be made negative semi-definite by proper tuning of the penalty parameters τ_{11} and τ_{12}. However, it can be shown (although not displayed here) that it is not possible to make $\tilde{R}_N$ negative semi-definite with only these two penalties.

By introducing the auxiliary variable $w \equiv v_t$, Eq. (4.16) can be re-written as

$$\begin{aligned} v_t &= w, \\ w_t &= 2aD_1 w + cD_1 D_1 v + SAT_2, \end{aligned} \tag{4.20}$$

where

$$SAT_2 = \tau_{11} H^{-1} e_N (w_N - g_{11}) + \tau_{12} H^{-1} e_N ((D_1 v)_N - g_{12}).$$

The reason for introducing the approach (4.20) is twofold, namely: 1) we would like to employ a Runge-Kutta method to time-advance the semi-discrete problem, and 2) we need to consider another penalty SAT_1 to turn $\tilde{R}_N$ negative semi-definite. The new penalty term is given by

$$SAT_1 = \tau_{13} H^{-1} D_1^T e_N ((D_1 v)_N - g_{12}),$$

and should be added to the first equation in the system (4.20); i.e., we obtain the modified problem

$$\begin{aligned} v_t &= w + SAT_1, \\ w_t &= 2aD_1 w + cD_1 D_1 v + SAT_2. \end{aligned} \tag{4.21}$$

The energy method on Eq. (4.21) leads to

$$\frac{d}{dt}(E_1)_H = x_N^T R_N x_N - x_0^T R_0 x_0 \equiv BT,$$

where, now,

$$R_N = \begin{bmatrix} a+2\tau_{11} & c-a\tau_{11}+\tau_{12} \\ c-a\tau_{11}+\tau_{12} & -ac-2a\tau_{12}+2\tau_{13} \end{bmatrix}. \tag{4.22}$$

Lemma 4.2. *The scheme* (4.21) *with homogeneous data is stable for $c<0$, if D_1 is a narrow-diagonal SBP operator, and $\tau_{11} = -a$, $\tau_{12} = 2c + a^2$, $\tau_{13} = -h^2 a$ hold.*

Proof. The energy method in combination with a more careful eigenvalue analysis (not shown here) show that the following parameter choice

$$\tau_{11}=-a, \quad \tau_{12}=2c+a^2, \quad \tau_{13}=-h^2a, \tag{4.23}$$

leads to non-positive eigenvalues for Eq. (4.21), provided that D_1 is a narrow-diagonal SBP operator. □

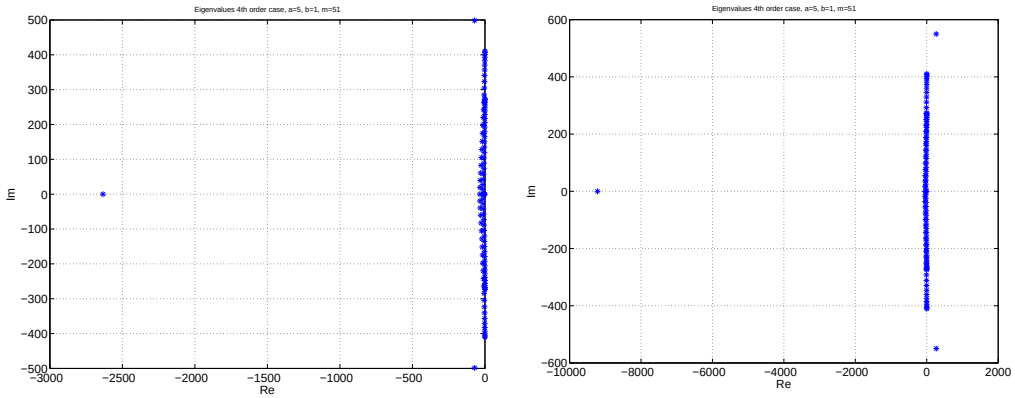

Figure 2: The eigenvalues to Eq. (4.21) for the fourth-order case, comparing a SBP closure (left) and a non-SBP closure (right). $b=1, a=5, N=51$.

In Fig. 2 we compare the eigenvalues to Eq. (4.21) for the fourth-order SBP and non-SBP cases, where $b=1, a=5, N=51$. (The penalty parameters are given by Eq. (4.23). The non-SBP operator is presented in [31] and is presented in Appendix for completeness). The largest real part of the eigenvalues is $-1.81\cdot10^{-10}$ for the SBP-SAT method. The corresponding non-SBP scheme results in eigenvalues with positive real part (the largest real part is 265.29), thus rendering the scheme unstable.

The main focus in the present study is to derive stability conditions for a semi-discretization of (2.6) using narrow-diagonal SBP operators D_1 and D_2. Consider the *pth* order accurate narrow-stencil approximation (compare with corresponding wide-stencil approximation Eq. (4.21))

$$\begin{aligned} v_t &= w + S\tilde{A}T_1 + \tilde{D}I_1 v, \\ w_t &= 2aD_1 w + cD_2 v + S\tilde{A}T_2 + \tilde{D}I_2 w, \end{aligned} \tag{4.24}$$

where

$$\begin{aligned} S\tilde{A}T_1 &= \tau_{13}H^{-1}S^T e_N((Sv)_N - g_{12}), \\ S\tilde{A}T_2 &= \tau_{11}H^{-1}e_N(w_N - g_{11}) + \tau_{12}H^{-1}e_N((Sv)_N - g_{12}). \end{aligned} \tag{4.25}$$

Here we have added two new operators:

$$\begin{aligned} \tilde{D}I_1 &= c\sigma_1 H^{-1}\tilde{R}^{(p)} + c\sigma_2 H^{-1}D_1^T\tilde{R}^{(p)}D_1, \\ \tilde{D}I_2 &= c\sigma_3 H^{-1}\tilde{R}^{(p)}, \end{aligned}$$

where $\tilde{R}^{(p)}$ is a dissipation operator (see Definition 3.5). Possible formulations of $\tilde{R}^{(p)}$ are given in Eq. (3.7).

Remark 4.1. The $S\tilde{A}T_1$ penalty in (4.24) introduces S^T, implying that the Neumann boundary condition will be imposed weakly at all points used in the reconstruction of the boundary derivative $(Sv)_N$. The boundary derivative approximation of the fourth-order accurate S operator (see Appendix) requires five points in the reconstruction. This means that the five points closest to the boundary will be penalized, with the weights given by the coefficients in S.

The first main result of this paper is stated in the following Lemma:

Lemma 4.3. *The pth-order accurate scheme* (4.24) *is stable if* D_1 *and* D_2 *are fully compatible,* $\sigma_1=\sigma_2=a$, $a\sigma_3=1$, *and Lemma* 4.2 *holds.*

Proof. By multiplying the first row in Eq. (4.21) by v^TH from the left and the second row by $w^TH-av^TQ^T$ and adding the transpose, we obtain

$$\frac{d}{dt}(E_1)_H=BT,$$

where BT corresponds to the boundary terms. By Lemma 4.2 BT is non-positive. For fully compatible *pth*-order accurate SBP operators, the following property holds: $D_2=D_1D_1-H^{-1}R^{(p)}$, where $R^{(p)}$ is positive semi-definite. This means that the energy method applied to Eq. (4.24) leads to

$$\frac{d}{dt}(E_1)_H=BT+cy^TAy,$$

where

$$y=\begin{bmatrix} v \\ D_1u \\ w \end{bmatrix}, \quad A=\begin{bmatrix} 2\sigma_1\tilde{R}^{(p)} & aR^{(p)} & -R^{(p)} \\ aR^{(p)} & 2\sigma_2\tilde{R}^{(p)} & -a\sigma_3\tilde{R}^{(p)} \\ -R^{(p)} & -a\sigma_3\tilde{R}^{(p)} & 2\sigma_3\tilde{R}^{(p)} \end{bmatrix}.$$

Since $\tilde{R}^{(p)}$ dominates $R^{(p)}$, the matrix A is positive semi-definite if

$$\tilde{A}=\begin{bmatrix} 2\sigma_1 & a & -1 \\ a & 2\sigma_2 & -a\sigma_3 \\ -1 & -a\sigma_3 & 2\sigma_3 \end{bmatrix}$$

is positive definite, which is true if $\sigma_1=\sigma_2=a$, $a\sigma_3=1$ hold. □

A more careful eigenvalue analysis (not presented here) reveals that we can use slightly less artificial dissipation to maintain strict stability. By using fully compatible SBP operators it is found that Eq. (4.24) is stable if

$$\sigma_2=0, \quad \sigma_1=\sigma_3=h. \tag{4.26}$$

Remark 4.2. A semi-discretization of (2.6) using a narrow-stencil approximation will require the addition of artificial dissipation also for the Cauchy problem. Possible formulations of $\tilde{R}^{(p)}$ are then given in Eq. (3.6).

In Fig. 3 we compare the eigenvalues to Eq. (4.24) for the sixth-order SBP and non-SBP cases, where $b=1, a=1.01, N=51$. The penalty parameters are given by Eq. (4.23), and the dissipation parameters are given by Eq. (4.26).

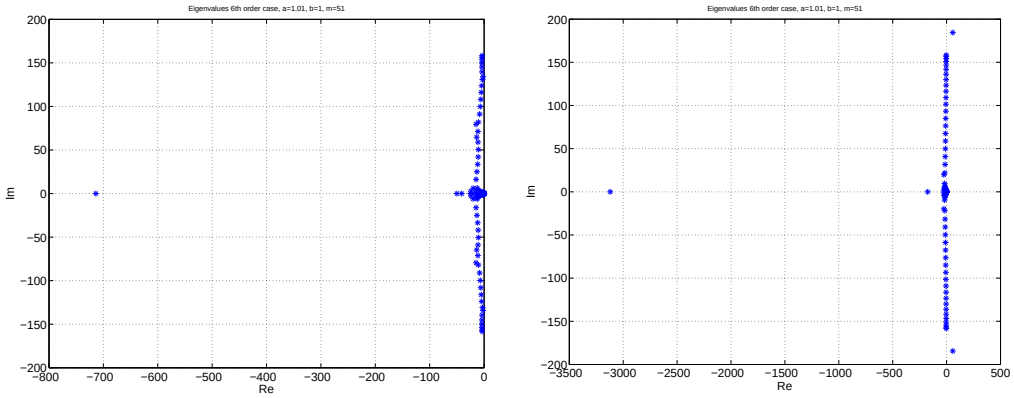

Figure 3: The eigenvalues to Eq. (4.24) for the sixth-order case, comparing a SBP closure (left) and a non-SBP closure (right). $b=1, a=1.01, N=51$.

The largest real part of the eigenvalues is $-7.83\cdot 10^{-13}$ for the SBP-SAT method. The corresponding non-SBP scheme results in eigenvalues with positive real part (the largest real part is 55.264), thus rendering the scheme unstable. (The only difference between the SBP and non-SBP implementations of (4.24) above is the difference operators $D_{1,2}$, i.e., the penalties $SAT_{1,2}$ and the dissipation operators $DI_{1,2}$ are kept identical to isolate the effect of the SBP closures).

Remark 4.3. The eigenvalue analysis (not presented here) reveals that stability of Eq. (4.21) and Eq. (4.24) are highly sensitive to slight deviations from the stability region of the penalty- and dissipation-parameters given by (4.23) and (4.26) respectively. This is also verified by the simulations done in Section 5. For example, if we set $\tau_{12}=(2c+a^2)\cdot 1.3$ instead of $\tau_{12}=2c+a^2$, the largest part of the eigenvalues becomes 0.34 instead of $-7.83\cdot 10^{-13}$ for the SBP-SAT method.

4.2 The non-constant coefficient 1-D problem

We will now modify the newly derived SBP-SAT technique to account for non-constant coefficients. We will limit the analysis to the two cases $c(x,t)>0$ and $c(x,t)<0$. A more suitable form of Eq. (2.6) is found by a time-splitting $(au_x)_t=a_tu_x+au_{xt}$, which yield the equivalent (to Eq. (2.6)) form

$$u_{tt}-a_tu_x-au_{xt}-(au_t)_x-((b-a^2)u_x)_x=0. \tag{4.27}$$

Case 1, $c>0$

Multiplying (4.27) by u_t and integrating by parts leads to

$$\frac{d}{dt}E_0 = 2u_t(au_t+cu_x)\big|_0^1 + RT_0, \tag{4.28}$$

where E_0 is the same as in (4.3) and the remaining terms are given by

$$RT_0 = \int_0^1 2a_t u_t u_x + c_t(u_x)^2 dx. \tag{4.29}$$

By applying the CBCs (4.6) we obtain

$$\frac{d}{dt}E_0 = BT_0 + RT_0, \tag{4.30}$$

where the boundary terms are given by $BT_0 = -2\sqrt{b}(u_{0t})^2 - 2\sqrt{b}(u_{1t})^2$. The inequality $2uv \le u^2+v^2$ gives

$$2a_t u_t u_x + c_t(u_x)^2 \le \left(\frac{|a_t|}{\sqrt{c}} + \frac{\sqrt{|c_t|}}{c}\right)((u_t)^2 + c(u_x)^2) \le K_0 E_0, \tag{4.31}$$

where K_0 is a constant. Integration of (4.30) leads to $(E_0)_t \le K_0 E_0 + BT_0$, so that

$$E_0 - \int_0^t BT_0 e^{K_0\tau} d\tau \le (E_0)_0 e^{K_0 t}, \tag{4.32}$$

with $(E_0)_0$ the initial energy.

Remark 4.4. The energy estimate (4.32) is not sharp. We have only a upper bound of K_0. By mimicking the energy estimate (4.30), the discrete approximation will mimic the time-growth of (4.32). If $a_t = c_t = 0$, $K_0 = 0$ and we can prove energy conservation.

Hence, compared to the constant coefficient case (4.7), there are potential time-growth situations, depending on a_t.

A semi-discretization of (4.27) using first-derivative SBP operators, and the SAT method to impose the CBCs (4.6), can be written as

$$v_{tt} - \bar{A}_t D_1 v - \bar{A} D_1 v_t - D_1 \bar{A} v_t - D_1 \bar{C} D_1 v = SAT_0 + SAT_1. \tag{4.33}$$

The matrices $\bar{A}$, $\bar{A}_t$ and $\bar{C}$ have the values of a, a_t and c injected on the diagonal. The penalty terms in Eq. (4.33) are identical to those in (4.9).

Lemma 4.4. *The energy method applied to* (4.33) *leads to an energy estimate that mimics* (4.30)*, if* $c(x,t)>0$*,* D_1 *is a narrow-diagonal SBP operator,* $\tau_0 = \lambda_2$ *and* $\tau_1 = -\lambda_1$*.*

Proof. Let $g_0=g_1=0$. Multiplying (4.33) by $v_t^T H$ from the left and adding the transpose leads to

$$\begin{aligned}&\frac{d}{dt}\Big(\|v_t\|_H^2+(D_1v)^T H\bar{C}(D_1v)\Big)\\ =&2(v_{0t})^2(-a+\tau_0)+2(v_{Nt})^2(a+\tau_1)-2(v_0)_t(D_1v)_0(c+\tau_0\lambda_1)\\ &+2(v_N)_t(D_1v)_N(c-\tau_1\lambda_2)+(D_1v)^T H\bar{C}_t(D_1v)+v_t^T\bar{A}_t HD_1v+v^T H\bar{A}_tD_1v_t.\end{aligned}$$

To obtain a non-growing energy requires $\tau_0=-c/\lambda_1\equiv\lambda_2$ and $\tau_1=c/\lambda_2\equiv-\lambda_1$, which inserted in the above expression yields

$$\begin{aligned}&\frac{d}{dt}\Big(\|v_t\|_H^2+(D_1v)^T H\bar{C}(D_1v)\Big)\\ =&-2\sqrt{b}(v_{0t})^2-2\sqrt{b}(v_{Nt})^2+(D_1v)^T H\bar{C}_t(D_1v)+v_t^T\bar{A}_t HD_1v+v^T H\bar{A}_tD_1v_t.\end{aligned}$$

This exactly mimics the continuous estimate (4.30). □

A narrow-stencil discretization of (4.27) using SBP operators requires the split form of the second-derivative term, i.e., $(cu_x)_x=c_xu_x+cu_{xx}$. As before we use the SAT method to impose the CBCs (4.6), and the resulting semi-discrete scheme can then be written as

$$v_{tt}-\bar{A}_tD_1v-\bar{A}D_1v_t-D_1\bar{A}v_t-\bar{C}_xD_1v-\bar{C}D_2v=SAT_0+SAT_1. \tag{4.34}$$

Lemma 4.5. *The energy method applied to* (4.34) *leads to an energy estimate that mimics* (4.30)*, if* $c(x,t)>0$*,* D_1 *and* D_2 *are fully compatible for* $c(x)>0$*,* $\tau_0=\lambda_2$ *and* $\tau_1=-\lambda_1$*.*

Proof. The proof follows directly from the proof of Lemma 4.4 and the fact that D_1 and D_2 are fully compatible, meaning that $\bar{C}_xD_1v+\bar{C}D_2v=-D_1\bar{C}D_1v-CH^{-1}R_c$, where R_c is positive semi-definite for $c(x)>0$. □

Case 1, $c<0$

Multiplication of Eq. (4.27) by u_t-au_x and integration by parts yield

$$\frac{d}{dt}E_1=\left(\frac{\lambda_1}{2}(u_t-\lambda_2u_x)^2+\frac{\lambda_2}{2}(u_t-\lambda_1u_x)^2\right)|_0^1+RT_1, \tag{4.35}$$

where E_1 is given by (4.5) and the remaining terms are

$$RT_1=\int_0^1(-(b_t+ac_x-a_xc)(u_x)^2+a_x(u_t)^2-2aa_xu_xu_t)\,dx. \tag{4.36}$$

By applying the boundary conditions (4.13) we obtain

$$\frac{d}{dt}E_1=BT_1+RT_1, \tag{4.37}$$

where the boundary terms are given by

$$BT_1 = -\left(\frac{\lambda_1}{2}(u_t-\lambda_2 u_x)^2+\frac{\lambda_2}{2}(u_t-\lambda_1 u_x)^2\right)|_{x=0}.$$

The inequality $2uv \le u^2+v^2$ leads to

$$\begin{aligned} &-(b_t+ac_x-a_xc)(u_x)^2+a_x(u_t)^2-2aa_xu_xu_t \\ &\le \left(a_x+\frac{|ac_x+b_2+2a^2a_x|}{b}\right)E_1 \le K_1E_1, \end{aligned} \tag{4.38}$$

where K_1 is a constant. Integration of (4.37) gives $(E_1)_t \le K_1E_1+BT_1$, so that

$$E_1-\int_0^t BT_1e^{K_1\tau}d\tau \le (E_1)_0e^{K_1t}, \tag{4.39}$$

with $(E_1)_0$ the initial energy. Hence, compared to the constant coefficient case (4.15), we face potential time-growth problems.

By introducing the auxiliary variable $w \equiv v_t$, a semi-discretization of (4.27) using only the first-derivative SBP operator D_1, and the SAT method to impose the boundary conditions (4.13), can be written as

$$\begin{aligned} v_t &= w+SAT_1, \\ w_t &= \bar{A}_tD_1v+\bar{A}D_1w+D_1\bar{A}w+D_1\bar{C}D_1v+SAT_2, \end{aligned} \tag{4.40}$$

where the penalty terms (which are identical to the constant coefficient case) are given by

$$\begin{aligned} SAT_1 &= \tau_{13}H^{-1}D_1^Te_N((D_1v)_N-g_{12}), \\ SAT_2 &= \tau_{11}H^{-1}e_N(w_N-g_{11})+\tau_{12}H^{-1}e_N((D_1v)_N-g_{12}). \end{aligned} \tag{4.41}$$

Lemma 4.6. *The pth-order accurate scheme* (4.40) *is stable if* D_1 *is a narrow-diagonal SBP operator and Lemma* 4.2 *holds.*

Proof. Multiplying the first equation in (4.40) by v^TH, and the second by $(w-\bar{A}D_1v)^TH$ from the left, and adding the transpose, leads to

$$\frac{d}{dt}(E_1)_H = BT+RT_H,$$

where the boundary term is $BT = x_N^TR_Nx_N-x_0^TR_0x_0$, with $x_{0,N}^T = [(w,(D_1v)]_{0,N}$ and the matrices R_N and R_0 are defined in (4.19) and (4.22). By Lemma 4.2 BT is non-positive. The discrete energy is given by

$$(E_1)_H = (\|w-\bar{A}D_1v\|_H^2+(D_1v)^TH\bar{B}(D_1v)), \tag{4.42}$$

while the remaining terms are

$$\begin{aligned} RT_H = &(Dv)^T(\bar{C}Q\bar{A}-\bar{A}Q\bar{C})D_1v-(D_1v)^TH(\bar{A}Q\bar{A}-\bar{A}^2Q)w \\ &-w(\bar{A}Q^T\bar{A}-Q^T\bar{A}^2)D_1v-(D_1v)^TH\bar{B}_tD_1v. \end{aligned} \tag{4.43}$$

The remaining terms RT_H can be shown to mimic the remaining terms (4.36) of the continuous case. □

Consider now the narrow-stencil approximation

$$\begin{aligned} v_t &= w+SAT_1+DI_1, \\ w_t &= \bar{A}_tD_1v+\bar{A}D_1w+D_1\bar{A}w+\bar{C}_xD_1v+\bar{C}D_2v+S\tilde{A}T_2+DI_2, \end{aligned} \tag{4.44}$$

where

$$\begin{aligned} DI_1 &= \sigma_1H^{-1}\tilde{R}_c^{(p)}+\sigma_2H^{-1}D_1^T\tilde{R}_c^{(p)}D_1, \\ DI_2 &= \sigma_3H^{-1}\tilde{R}_c^{(p)}. \end{aligned} \tag{4.45}$$

Possible formulations of $\tilde{R}_c^{(p)}$ are given in Eq. (3.8).

The following lemma is the extension of Lemma 4.3 to the variable coefficient case:

Lemma 4.7. *The pth-order accurate scheme* (4.44) *is stable if* D_1 *and* D_2 *are fully compatible for* $c(x)>0$, *and Lemma* 4.3 *hold.*

We omit the proof, since it is completely analogous to the proof of Lemma 4.3.

The eigenvalues of Eq. (4.44) using the fully compatible sixth-order accurate SBP operators for two different cases are presented in Fig. 4. In the first case $b=1, a=1.5+0.1cos(4\pi x), N=51$ (corresponding to case 2 in Section 5). In the second case $b=1, a=1.2+0.3cos(4\pi x), N=51$ (corresponding to case 3 in Section 5).

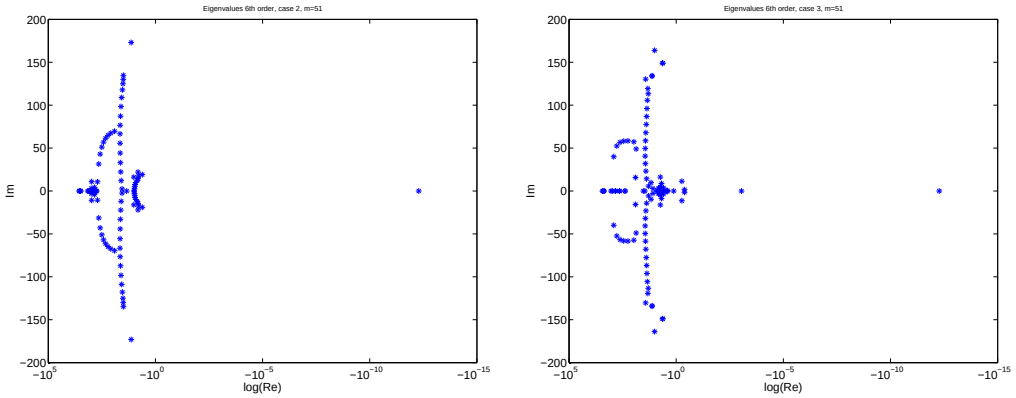

Figure 4: The eigenvalues to Eq. (4.44) for the sixth-order case, comparing two different settings with $b=1, N=51$ and: $a=1.5+0.1cos(4\pi x)$ (left), $a=1.2+0.3cos(4\pi x)$ (right).

5 Computations

To test the accuracy of the newly developed SBP-SAT technique, we perform numerical simulations of the variable coefficient equation (2.6). Three different cases are tested, namely: 1) $c>0$, 2) $c<0$ everywhere, and 3) $c<0$ at the boundaries, and changing sign in the interior. We have implemented a mechanism by which the dissipative operator is "switched on" whenever $c<0$.

To further elucidate the favorable stability and accuracy properties of a narrow-stencil approximation compared to the corresponding wide-stencil approximation we will compare each result using both schemes (wide and narrow). In the first test we compare accuracy. In the second test we compare the stability properties when the solution is non-smooth (corresponding to case 3 below).

For the time integration we use the standard explicit fourth-order Runge-Kutta method. The time-step is kept small enough not to interfere with the spatial discretization error (dt/dx is roughly 0.04, for the chosen parameter setting.) The normalized initial data used in the computations (we chose highly smooth functions, to keep the errors derived from lack of smoothness to the minimum) is given by:

$$\begin{aligned} &u(t=0)=1.099\times 10^{12}\,(x-0.25)^{10}(x-0.75)^{10}, && \text{for } x\in[0.25,0.75],\\ &u(t=0)=0, && \text{otherwise;}\\ &u_t(t=0)=0. \end{aligned}$$

We use homogeneous boundary conditions (i.e. $g_0=g_1=0$) in all cases.

The convergence rate is calculated as

$$Q=\log\left(\frac{\|v-v^{(h_1)}\|_{l_2}}{\|v-v^{(h_2)}\|_{l_2}}\right)/\log(h_1/h_2), \tag{5.1}$$

where $v^{(h_i)}$ is the numerical solution with grid spacing h_i and v is a numerical solution calculated for an extremely fine resolution (N=1601) which can, for every practical purpose, be considered as the "exact solution" (since we have stability proofs). The discrete l_2-error for a given grid size h is obtained as $\|v-v^{(h)}\|_{l_2}$. In all the cases, except the last case, the l_2-error is recorded at $t=0.4$ (for the last case, the evaluation is made at $t=0.24$, for reasons that will become clear later). For simplicity and without loose of generalization, we set $b=1$, so that the function c is completely determined by the shift a.

Case 1, $c>0$ **at the boundary**

In this case, the penalty operators are given just below Eq. (4.9). We chose $a(x)=0.5cos(2\pi x)$, which yields $c>0$ in the whole domain. Convergence studies for the second-, fourth- and sixth-order accurate narrow-stencil approximations are shown in Table 1. The corresponding results using second-, fourth- and sixth-order accurate wide-stencil approximations are show in Table 2.

Table 1: $\log(l_2-errors)$, and convergence rates for the second-, fourth- and sixth-order narrow-stencil approximations of the shifted wave equation for case 1 ($c>0$).

N	$\log l_2^{(2)}$	$Q^{(2)}$	$\log l_2^{(4)}$	$Q^{(4)}$	$\log l_2^{(6)}$	$Q^{(6)}$
101	-2.77		-3.97		-3.78	
201	-3.38	2.04	-5.16	3.93	-6.07	7.62
401	-3.99	2.01	-6.35	3.95	-7.95	6.24
801	-4.59	2.00	-7.55	3.99	-9.80	6.14

Table 2: $\log(l_2-errors)$, and convergence rates for the second-, fourth- and sixth-order wide-stencil approximations of the shifted wave equation for case 1 ($c>0$).

N	$\log l_2^{(2)}$	$Q^{(2)}$	$\log l_2^{(4)}$	$Q^{(4)}$	$\log l_2^{(6)}$	$Q^{(6)}$
101	-1.90		-3.00		-3.39	
201	-2.48	1.95	-4.18	3.92	-5.38	6.60
401	-3.09	2.00	-5.38	3.98	-7.24	6.18
801	-3.69	2.00	-6.58	3.99	-8.74	5.01

The evolution of the pulse is displayed in Fig. 5.

The convergence results in Tables 1-2 are consistent with theory (see [36] for more information on the accuracy of finite difference approximations) except for the sixth-order case (narrow-stencil) which shows one order higher than the expected fifth-order convergence. By comparing Table 1 and Table 2 the gain of using a narrow-stencil approximation for this case is evident.

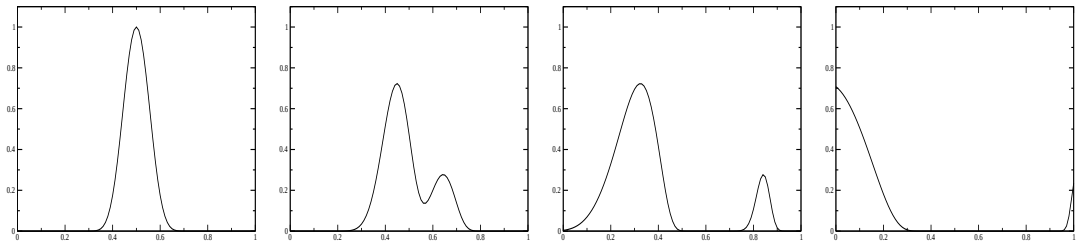

(a) $t=0$ (b) $t=0.1$ (c) $t=0.3$ (d) $t=0.6$

Figure 5: Evolution of the initial pulse for different instants of time, case 1.

Case 2, $c<0$ in the whole domain

For this case, we use $a(x)=1.5+0.1cos(4\pi x)$ such that c is negative in the whole domain, including the boundaries (hence the appropriate SAT treatment is given by (4.41)). Convergence studies for the nth-order accurate narrow-stencil approximation ($n=2,4,6$) are presented in Table 3. The corresponding results using second-, fourth- and sixth-order accurate wide-stencil approximations are show in Table 4.

The convergence results in Table 3 show that the sixth-order method yields a convergence closer to seven (as compared to the expected fifth-order convergence). We have

Table 3: $\log(l_2-errors)$, and convergence rates for the second-, fourth- and sixth-order narrow-stencil approximations of the shifted wave equation for case 2 ($c<0$).

N	$\log l_2^{(2)}$	$Q^{(2)}$	$\log l_2^{(4)}$	$Q^{(4)}$	$\log l_2^{(6)}$	$Q^{(6)}$
101	-1.67		-2.73		-3.19	
201	-2.38	2.37	-4.14	4.68	-5.19	6.64
401	-3.08	2.32	-5.52	4.57	-7.28	6.93
801	-3.80	2.39	-6.81	4.29	-9.35	6.88

Table 4: $\log(l_2-errors)$, and convergence rates for the second-, fourth- and sixth-order wide-stencil approximations of the shifted wave equation for case 2 ($c<0$).

N	$\log l_2^{(2)}$	$Q^{(2)}$	$\log l_2^{(4)}$	$Q^{(4)}$	$\log l_2^{(6)}$	$Q^{(6)}$
101	-1.81		-3.18		-3.50	
201	-2.41	1.99	-4.31	3.77	-4.66	3.85
401	-3.01	2.00	-5.35	3.45	-5.63	3.20
801	-3.61	2.00	-6.23	2.92	-6.54	3.04

no explanation to this super-convergence behavior. For this case the gain (in accuracy) using a narrow-stencil approximation is clearly seen for the sixth-order case, but not as clear for the second- and fourth-order cases.

The evolution of the pulse is displayed in Fig. 6.

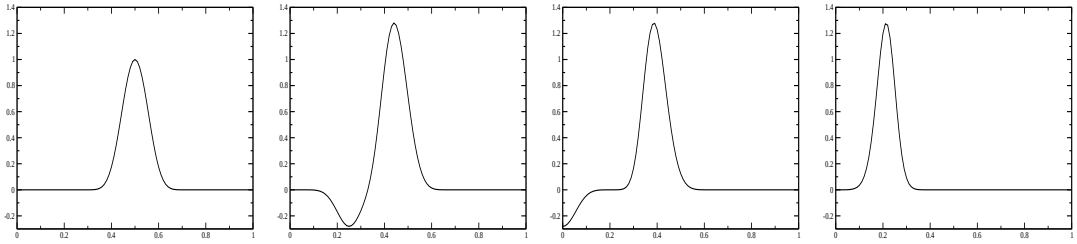

(a) $t=0$ (b) $t=0.1$ (c) $t=0.2$ (d) $t=0.6$

Figure 6: Evolution of the initial pulse for different instants of time, case 2.

Case 3, $c<0$ at the boundary, changing sign in the interior

In the last case we study the effect of c changing sign, testing the artificial dissipation mechanism implemented in the code, namely, a method by which the artificial dissipation is "switched on" whenever $c<0$. We set $a(x)=1.2+0.3\cos(4\pi x)$, leading to a c that is negative at both boundaries (so the SAT treatment is given by (4.41)), and changes sign four times in the interior. Convergence studies for the nth-order accurate narrow-stencil approximations ($n=2,4,6$) are shown in Table 5. The results using the corresponding wide-stencil approximations are shown in Table 6.

The $l_2-errors$ are now recorded at $t=0.24$ (instead of $t=0.4$ used for the previous cases). The reason for this is that the solution yields an increasing sharpness of the peak

Table 5: $\log(l_2-errors)$, and convergence rates for the second-, fourth- and sixth-order narrow-stencil approximations of the shifted wave equation for case 3 ($c<0$ at the boundary, changing sign in the interior).

N	$\log l_2^{(2)}$	$Q^{(2)}$	$\log l_2^{(4)}$	$Q^{(4)}$	$\log l_2^{(6)}$	$Q^{(6)}$
101	-1.87		-2.73		-2.85	
201	-2.56	2.29	-4.08	4.47	-4.60	5.81
401	-3.23	2.23	-5.50	4.74	-6.65	6.82
801	-3.94	2.34	-6.81	4.33	-8.73	6.89

Table 6: $\log(l_2-errors)$, and convergence rates for the second-, fourth- and sixth-order wide-stencil approximations of the shifted wave equation for case 3 ($c<0$ at the boundary, changing sign in the interior).

N	$\log l_2^{(2)}$	$Q^{(2)}$	$\log l_2^{(4)}$	$Q^{(4)}$	$\log l_2^{(6)}$	$Q^{(6)}$
101	-2.00		-3.20		-3.64	
201	-2.62	2.06	-4.36	3.85	-4.84	3.99
401	-3.23	2.04	-5.48	3.70	-6.03	3.97
801	-3.84	2.01	-6.50	3.41	-7.24	3.99

(see Fig. 7). After $t\sim 0.25$ one of the modes starts to "pile up" (this happens at a point where c changes sign and therefore the mode with eigenvalue $\lambda_2=a-\sqrt{b}$ has vanishing velocity). At t=5 the pulse has transformed into a step function with decreasing amplitude.

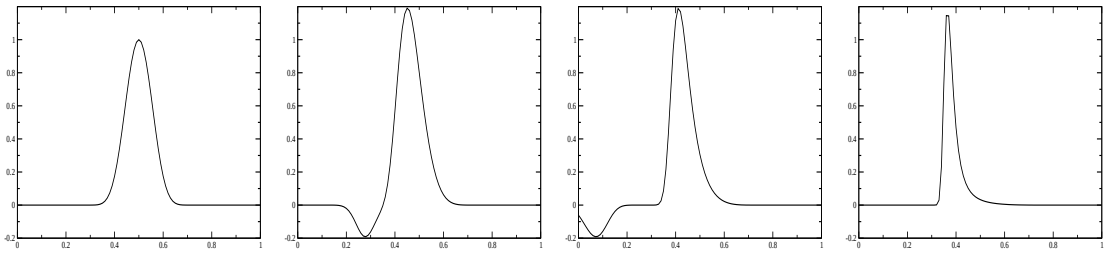

(a) $t=0$ (b) $t=0.1$ (c) $t=0.2$ (d) $t=0.4$

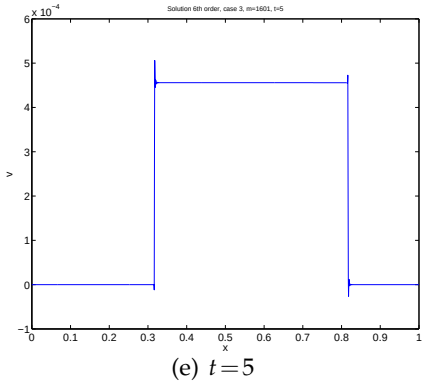

(e) $t=5$

Figure 7: Evolution of the initial pulse for different instants of time, using the sixth-order accurate narrow-stencil formulation and $N=1601$ for case 3. Notice the increasing (with time) sharpness of the pulse.

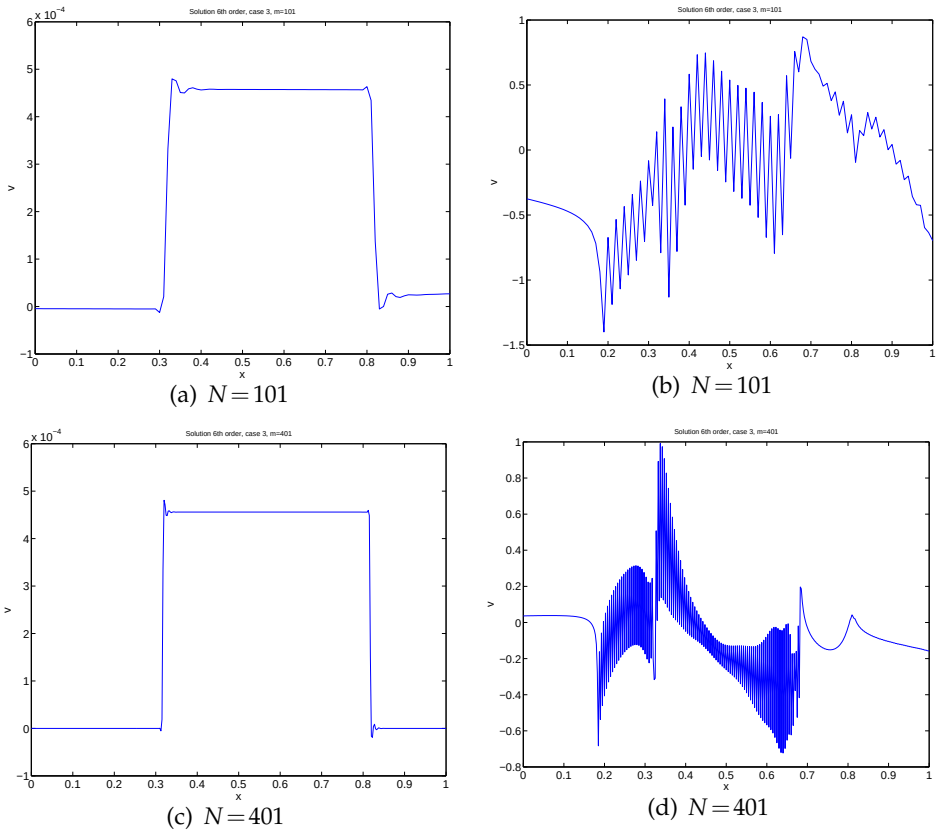

(a) $N=101$ (b) $N=101$

(c) $N=401$ (d) $N=401$

Figure 8: Solution at $t=5$, comparing the sixth-order accurate narrow-stencil (left column) and wide-stencil (right column) formulations for case 3. Spurious oscillations are present (right column).

To capture this solution using much less (than $N=1601$) grid-points is a challenging problem, without the introduction of a shock-capturing technique. (That is however out of the scope of the present study.). The leading motives in [22] of using a narrow-stencil approximation was to have: 1) natural damping of the highest frequency mode, and 2) more accurate approximations. The spurious oscillations are often triggered by unresolved features in the solution (like a shock).

In Fig. 8 comparison is done between the sixth-order accurate narrow- and wide-stencil SBP-SAT methods using $N=101$ and $N=401$ grid-points. The wide-stencil approximation clearly cannot capture this solution and leads to an unstable solution. The corresponding narrow-stencil approximation have no difficulty capturing this solution, even with as few as $N=101$ grid-points. The wide-stencil approximations clearly need artificial dissipation (AD) to damp the highest frequency mode. However, the addition of AD can easily destroy the stability properties of the original scheme when $c<0$ (see the remark at the end of Section 2 concerning the sensitivity of the penalty- and dissipation-parameters, to obtain stability).

6 Conclusions and future work

We have proven that narrow-stencil approximations of the shifted wave equation written on second-order form are strictly stable, if the first- and second-derivative finite difference operators are fully compatible, and a suitable amount of artificial dissipation is added. Our approach has been to use SBP operators and the SAT technique to enforce the boundary conditions. We have seen that the penalty (SAT) operators needed to implement these conditions must be carefully chosen for $c<0$ at the boundaries.

The numerical code developed using the above mentioned SBP-SAT method leads to time evolution that faithfully reproduces the physical behavior of the wave, and has the desired accuracy, both for the constant and the variable coefficient cases, especially for the difficult case where $c<0$ at the boundaries and changing sign in between (corresponding to case 3 in Section 5).

The more complex case of time-dependent coefficients will be dealt with in a coming study. The case where c changes sign in the interior performs with the expected order of accuracy (except the sixth-order case which yield super-convergence) and leads to a stable evolution. At later times the solution has an increasingly sharp gradient, but the code resolves this quite nice.

It is of outmost importance to have a stable scheme for situations where $c<0$, which would correspond to a region inside the event horizon. The present study is the first step towards a code that will make it possible to derive a strictly-stable narrow-stencil approximation to the full non-linear 3-D problem inside (and outside of) the event horizon.

The present technique can be extended to the full non-linear 3-D problem. With this in mind, the present study can be regarded as the first step towards a high-order accurate numerical formulation of Einstein´s Equations written in second-order form, with the aim of simulating processes such as binary black holes and neutron star collisions. Notice also that, to address many of the more challenging (interesting) problems, will require a multi-block approach (see for example [15, 20]) in combination with an adaptive grid method (see for example [30]), to efficiently capture all the relevant solution features. These issues will be the grounds for future work.

Acknowledgments

We wish to thank Oscar Reula for his invaluable help and various insightful comments. This work was supported in part by research funds of the National University of Córdoba. F.P. is supported by CONICET through a Post-doctoral grant.

Appendix: Fully compatible SBP operators

We now present the specific form of the fully compatible SBP operators used in the analysis. We consider the second-, fourth- and sixth-order accurate discretizations.

Second-order accurate case. For the second-order case we get

$$D_2 = H^{-1}(-D^T R D + BS),$$

where

$$D_2 = \frac{1}{h^2}\begin{bmatrix} 0 & 0 & 0 & & \\ 1 & -2 & 1 & & \\ & \ddots & \ddots & \ddots & \\ & & 1 & -2 & 1 \\ & & 0 & 0 & 0 \end{bmatrix}, \quad S = \frac{1}{h}\begin{bmatrix} -1 & 1 & & & \\ & 1 & & & \\ & & \ddots & & \\ & & & 1 & \\ & & & -1 & 1 \end{bmatrix},$$

$$D = \frac{1}{h}\begin{bmatrix} -1 & 1 & & & \\ & -1 & 1 & & \\ & & \ddots & & \\ & & & -1 & 1 \\ & & & -1 & 1 \end{bmatrix},$$

and

$$H = h \times diag\Big(\frac{1}{2}, 1, \cdots, 1, \frac{1}{2}\Big),$$
$$R = h \times diag(1, 1, \cdots, 1, 0).$$

For the second-order case we have also shown that we can use this factorization to construct a narrow-diagonal second-derivative operator for variable coefficient $(cu_x)_x$ terms. The form is then given by

$$D_2 = H^{-1}(-D^T \tilde{C} D + BS),$$

where C is given by Definition 3.3 and

$$\tilde{C} = \frac{h}{2} \times diag(a_0 + a_1, a_1 + a_2, \cdots, a_{N-1} + a_N, 0).$$

This yields a second-order accurate narrow-diagonal variable coefficient SBP operator.

Fourth-order accurate case. Fully compatible SBP operators, i.e.,

$$D_2 = D_1 D_1 - H^{-1} R, \quad R > 0.$$

The discrete norm is given by

$$H = h \times diag\Big(\frac{4567}{14400}, \frac{799}{576}, \frac{913}{1440}, \frac{1769}{1440}, \frac{2659}{2880}, \frac{14543}{14400}, 1, \cdots\Big).$$

The left boundary closure of Q is given by:

$$
\begin{aligned}
q_{1,1} &= -\tfrac{1}{2} & q_{1,6} &= 0 & q_{3,4} &= \tfrac{41}{480} & q_{5,6} &= \tfrac{26461}{43200} \\
q_{1,2} &= \tfrac{27029}{43200} & q_{2,3} &= \tfrac{2219}{8640} & q_{3,5} &= \tfrac{4963}{17280} & q_{5,7} &= -\tfrac{1}{12} \\
q_{1,3} &= \tfrac{373}{28800} & q_{2,4} &= \tfrac{10907}{17280} & q_{3,6} &= -\tfrac{1481}{14400} & q_{6,7} &= \tfrac{2}{3} \\
q_{1,4} &= -\tfrac{3169}{14400} & q_{2,5} &= -\tfrac{7}{24} & q_{4,5} &= \tfrac{3907}{8640} & q_{6,8} &= -\tfrac{1}{12} \\
q_{1,5} &= \tfrac{7037}{86400} & q_{2,6} &= \tfrac{2533}{86400} & q_{4,6} &= \tfrac{1277}{28800}
\end{aligned}
$$

In the interior we have the skew-symmetric stencil

$$(Qv)_j = \frac{1}{12}v_{j-2} - \frac{2}{3}v_{j-1} + \frac{2}{3}v_{j+1} - \frac{1}{12}v_{j+2}.$$

The left boundary closure of hM is given by

$$
\begin{aligned}
m_{1,1} &= \tfrac{87496510545979633426458011 83}{75560660040620398972307904 00} & m_{3,4} &= -\tfrac{33487027281694083150505 3}{20989072233505666381196 64} \\
m_{1,2} &= -\tfrac{11806166876130677741419781 81}{94450825050775498715384880 0} & m_{3,5} &= -\tfrac{22013116152419154133388103 1}{75560660040620398972307904 0} \\
m_{1,3} &= -\tfrac{18883688819587215872115121}{12593443340103399828717984 00} & m_{3,6} &= \tfrac{65250296322637253690816237}{94450825050775498715384880 0} \\
m_{1,4} &= \tfrac{13985831927735746206505543 3}{94450825050775498715384880 0} & m_{4,4} &= \tfrac{60219204209698597256358052 7}{37780330020310199486153952 0} \\
m_{1,5} &= -\tfrac{31028197499475755079772847 3}{75560660040620398972307904 00} & m_{4,5} &= -\tfrac{16999664383088213690051020 3}{18890165010155099743076976 0} \\
m_{1,6} &= 0 & m_{4,6} &= -\tfrac{56820203658905657689306769}{12593443340103399828717984 00} \\
m_{2,2} &= \tfrac{12374190000790967152792384 9}{55970859289348443683191040} & m_{5,5} &= \tfrac{10967296574653742683153196 33}{50373773360413599314871936 0} \\
m_{2,3} &= -\tfrac{95388620876161928526271007}{18890165010155099743076976 0} & m_{5,6} &= -\tfrac{11565760710703113505245931 69}{94450825050775498715384880 0} \\
m_{2,4} &= -\tfrac{48163874388288727322176144 7}{75560660040620398972307904 0} & m_{5,7} &= \tfrac{1}{12} \\
m_{2,5} &= \tfrac{30905226730185255587249 97}{15741804175129249785897480} & m_{6,6} &= \tfrac{18628351534348955410397982047}{75560660040620398972307904 00} \\
m_{2,6} &= -\tfrac{11174160933657881805343797 7}{75560660040620398972307904 0} & m_{6,7} &= -\tfrac{4}{3} \\
m_{3,3} &= \tfrac{34068445973829024067570011 1}{37780330020310199486153952 0} & m_{6,8} &= \tfrac{1}{12}
\end{aligned}
$$

In the interior we have the symmetric scheme:

$$h(Mv)_j = \frac{1}{12}v_{j-2} - \frac{4}{3}v_{j-1} + \frac{5}{2}v_j - \frac{4}{3}v_{j+1} + \frac{1}{12}v_{j+2}.$$

The fourth-order accurate boundary derivative operator is given by:

$$BS = \frac{1}{h}\begin{bmatrix} \frac{7200}{4567} & -\frac{27029}{13701} & -\frac{373}{9134} & \frac{3169}{4567} & -\frac{7037}{27402} & \\ & & 0 & & & \\ & & & \ddots & & \end{bmatrix}.$$

The fourth-order accurate non-SBP operator. In this case, we have

$$D_1=\frac{1}{h}\begin{bmatrix} -11 & 18 & -9 & 2 & & \\ -2 & -3 & 6 & -1 & & \\ \frac{1}{12} & -\frac{2}{3} & 0 & \frac{2}{3} & -\frac{1}{12} & \\ & \ddots & \ddots & \ddots & \ddots & \ddots \end{bmatrix}.$$

The sixth-order accurate non-SBP operators. In this case, we have

$$D_1=\frac{1}{60h}\begin{bmatrix} -147 & 360 & -450 & 400 & -225 & 72 & -10 \\ -10 & -77 & 150 & -100 & 50 & -15 & 2 \\ 2 & -24 & -35 & 80 & -30 & 8 & -1 \\ -1 & 9 & -45 & 0 & 45 & -9 & 1 \\ & \ddots & \ddots & \ddots & \ddots & \ddots & \ddots \end{bmatrix},$$

$$D_2=\frac{1}{h^2}\begin{bmatrix} \frac{114170}{40947} & -\frac{438107}{54596} & \frac{336409}{40947} & -\frac{276997}{81894} & \frac{3747}{13649} & \frac{21035}{163788} & & & & & \\ \frac{6173}{5860} & \frac{-2066}{879} & \frac{3283}{1758} & \frac{-303}{293} & \frac{2111}{3516} & \frac{-601}{4395} & & & & & \\ \frac{-52391}{81330} & \frac{134603}{32532} & \frac{-21982}{2711} & \frac{112915}{16266} & \frac{-46969}{16266} & \frac{30409}{54220} & & & & & \\ \frac{68603}{321540} & \frac{-12423}{10718} & \frac{112915}{32154} & \frac{-75934}{16077} & \frac{53369}{21436} & \frac{-54899}{160770} & \frac{48}{5359} & & & & \\ \frac{7053}{39385} & \frac{86551}{94524} & \frac{-46969}{23631} & \frac{53369}{15754} & \frac{-87904}{23631} & \frac{820271}{472620} & \frac{-1296}{7877} & \frac{96}{7877} & & & \\ \frac{21035}{525612} & \frac{-24641}{131403} & \frac{30409}{87602} & \frac{-54899}{131403} & \frac{820271}{525612} & \frac{-117600}{43801} & \frac{64800}{43801} & \frac{-6480}{43801} & \frac{480}{43801} & & \\ & & & \frac{1}{90} & \frac{-3}{20} & \frac{3}{2} & \frac{-49}{18} & \frac{3}{2} & \frac{-3}{20} & \frac{1}{90} & \\ & & & & \ddots & \ddots & \ddots & \ddots & \ddots & \ddots & \end{bmatrix}.$$

The sixth-order accurate case. Fully compatible SBP operators, i.e.,

$$D_2=D_1D_1-H^{-1}R,\quad R>0.$$

The left boundary closure for the norm is given by:

$$H=diag\Big(\frac{7493827}{25401600},\frac{5534051}{3628800},\frac{104561}{403200},\frac{260503}{145152},\frac{43237}{103680},\frac{514081}{403200},\frac{3356179}{3628800},\frac{25631027}{25401600}\Big).$$

The left boundary closure of Q is given by:

$$
\begin{aligned}
q_{1,1} &= -\tfrac{1}{2} & q_{2,3} &= \tfrac{3554293}{21772800} & q_{3,6} &= \tfrac{88913}{403200} & q_{5,7} &= \tfrac{654643}{3110400} \\
q_{1,2} &= \tfrac{144243419}{217728000} & q_{2,4} &= \tfrac{13951541}{21772800} & q_{3,7} &= -\tfrac{2877293}{21772800} & q_{5,8} &= -\tfrac{1158071}{16934400} \\
q_{1,3} &= -\tfrac{100087}{6096384} & q_{2,5} &= \tfrac{885133}{4838400} & q_{3,8} &= \tfrac{1810337}{60963840} & q_{6,7} &= \tfrac{59430457}{108864000} \\
q_{1,4} &= -\tfrac{3349159}{16934400} & q_{2,6} &= -\tfrac{54569873}{108864000} & q_{4,5} &= \tfrac{31487}{145152} & q_{6,8} &= -\tfrac{5026031}{152409600} \\
q_{1,5} &= -\tfrac{8487881}{152409600} & q_{2,7} &= \tfrac{24209}{129600} & q_{4,6} &= \tfrac{3410983}{5443200} & q_{6,9} &= -\tfrac{1}{60} \\
q_{1,6} &= \tfrac{49651253}{304819200} & q_{2,8} &= -\tfrac{1}{100} & q_{4,7} &= -\tfrac{911107}{4838400} & q_{7,8} &= \tfrac{30506159}{43545600} \\
q_{1,7} &= -\tfrac{111}{2000} & q_{3,4} &= \tfrac{9146267}{43545600} & q_{4,8} &= -\tfrac{338713}{152409600} & q_{7,9} &= -\tfrac{3}{20} \\
q_{1,8} &= 0 & q_{3,5} &= -\tfrac{140959}{777600} & q_{5,6} &= \tfrac{906379}{43545600} & q_{7,10} &= \tfrac{1}{60}
\end{aligned}
$$

In the interior we have the skew-symmetric stencil

$$(Qv)_j = -\frac{1}{60}v_{j-3} + \frac{3}{20}v_{j-2} - \frac{3}{4}v_{j-1} + \frac{3}{4}v_{j+1} - \frac{3}{20}v_{j+2} + \frac{1}{60}v_{j+3}.$$

The left boundary closure of hM is given by:

$$
\begin{aligned}
m_{1,1} &= 1.2000574331050846310 & m_{3,3} &= 1.6154560822068650044 \\
m_{1,2} &= -1.3493191282870869603 & m_{3,4} &= -1.9194919233346676031 \\
m_{1,3} &= 0.070178887841234707543 & m_{3,5} &= 1.5610425124000178977 \\
m_{1,4} &= 0.069590525249539236244 & m_{3,6} &= -0.90541517327846378866 \\
m_{1,5} &= 0.067470908000967733967 & m_{3,7} &= 0.29650034382549239075 \\
m_{1,6} &= -0.078177900310564991388 & m_{3,8} &= -0.041710318484992597153 \\
m_{1,7} &= 0.020199274400825642921 & m_{4,4} &= 4.4952269369790344874 \\
m_{1,8} &= 0 & m_{4,5} &= -3.1817949974047985393 \\
m_{2,2} &= 2.3771262429420204291 & m_{4,6} &= 1.0808018521848171469 \\
m_{2,3} &= -0.67656041117548601149 & m_{4,7} &= -0.45961997566890306308 \\
m_{2,4} &= -0.17119675741265170011 & m_{4,8} &= 0.086484339407630035030 \\
m_{2,5} &= -0.49114472782781516546 & m_{5,5} &= 3.7441205742402132321 \\
m_{2,6} &= 0.41999078952455211907 & m_{5,6} &= -2.2187585468457396535 \\
m_{2,7} &= -0.11648186968013573680 & m_{5,7} &= 0.60169480955006113403 \\
m_{2,8} &= 0.0075858619166030259199 & m_{5,8} &= -0.082630532112906639616
\end{aligned}
$$

$$
\begin{aligned}
m_{6,6} &= 3.3035989548189179514 & m_{7,9} &= \tfrac{3}{20} \\
m_{6,7} &= -1.7308643575320354723 & m_{7,10} &= -\tfrac{1}{90} \\
m_{6,8} &= 0.13993549254962779959 & m_{8,8} &= 2.6996599266341938109 \\
m_{6,9} &= -\tfrac{1}{90} & m_{8,9} &= -\tfrac{3}{2} \\
m_{7,7} &= 2.6978965450148505391 & m_{8,10} &= \tfrac{3}{20} \\
m_{7,8} &= -1.4482136587990443235 & m_{8,11} &= -\tfrac{1}{90}
\end{aligned}
$$

In the interior we have the symmetric scheme:

$$
-h(Mv)_j = \frac{1}{90}v_{j-3} - \frac{3}{20}v_{j-2} + \frac{3}{2}v_{j-1} - \frac{49}{18}v_j + \frac{3}{2}v_{j+1} - \frac{3}{20}v_{j+2} + \frac{1}{90}v_{j+3}
$$

The fourth-order accurate boundary derivative operator is given by:

$$
BS = \begin{bmatrix}
\frac{12700800}{7493827} & -\frac{1009703933}{449629620} & \frac{2502175}{44962962} & \frac{913407}{1362514} & \frac{8487881}{44962962} & -\frac{49651253}{89925924} & \frac{7048944}{37469135} \\
 & & & 0 & & & \\
 & & & & \ddots & &
\end{bmatrix}.
$$

References

[1] S. Abarbanel and A. Ditkowski. Asymptotically stable fourth-order accurate schemes for the diffusion equation on complex shapes. J. Comput. Phys., 133:279–288, 1997.

[2] M. C. Babiuc, B. Szilagyi, and J. W Winicour. Harmonic initial-boundary evloution in general relativity. Physical Review D, 73:064017, 2006.

[3] A. Bayliss, K. E. Jordan, B. J. Lemesurier, and E. Turkel. A fourth order accurate finite difference scheme for the computation of elastic waves. Bull. Seismol. Soc. Amer., 76(4):1115–1132, 1986.

[4] G. Calabrese. Finite differencing second order systems describing black holes. Physical Review D, 71:027501, 2005.

[5] M. H. Carpenter, D. Gottlieb, and S. Abarbanel. Time-stable boundary conditions for finite-difference schemes solving hyperbolic systems: Methodology and application to high-order compact schemes. J. Comput. Phys., 111(2), 1994.

[6] P. Diener, E. N. Dorband, E. Schnetter, and M. Tiglio. Optimized high-order derivative and dissipation operators satisfying summation by parts, and applications in three-dimensional multi-block evolutions. J. Sci. Comput., 32(1):109–145, 2007.

[7] A. E. Fisher and J. E. Marsden. The einstein evolution equations as a first-order quasi-linear symmetric hyperbolic system, i. Commun. Math. Phys., 28:1–38, 1972.

[8] B. Gustafsson, H.-O. Kreiss, and J. Oliger. Time dependent problems and difference methods. John Wiley & Sons, Inc., 1995.

[9] B. Gustafsson, H.-O. Kreiss, and A. Sundström. Stability theory of difference approximations for mixed initial boundary value problems. Math. Comp., 26(119), 1972.

[10] B. Gustafsson and P. Olsson. Fourth-order difference methods for hyperbolic IBVPs. J. Comput. Phys., 117(1), 1995.

[11] J. S. Hesthaven. A stable penalty method for the compressible Navier-Stokes equations: II Multi-dimensional domain decomposition schmemes. SIAM J. Sci. Comput., 1998.
[12] H.-O. Kreiss, N. A. Petersson, and J. Yström. Difference approximations for the second order wave equation. SIAM J. Num. Anal., 40:1940–1967, 2002.
[13] H.-O. Kreiss and G. Scherer. Finite Element and Finite Difference Methods for Hyperbolic Partial Differential Equations. Mathematical Aspects of Finite Elements in Partial Differential Equations., Academic Press, Inc., 1974.
[14] H.-O. Kreiss and J. Oliger. Comparison of accurate methods for the integration of hyperbolic equations. Tellus XXIV, 3, 1972.
[15] L. Lehner, O. Reula, and M. Tiglio. Multi-block simulations in general relativity: high-order discretizations, numerical stability and applications. Classical Quantum Gravity, 22:5283–5321, 2005.
[16] S. K. Lele. Compact finite difference schemes with spectral-like resolution. J. Comput. Phys., 103:16–42, 1992.
[17] K. Mattsson, F. Ham, and G. Iaccarino. Stable and accurate wave propagation in discontinuous media. J. Comput. Phys., 227:8753–8767, 2008.
[18] K. Mattsson and J. Nordström. Summation by parts operators for finite difference approximations of second derivatives. J. Comput. Phys., 199(2):503–540, 2004.
[19] K. Mattsson and J. Nordström. High order finite difference methods for wave propagation in discontinuous media. J. Comput. Phys., 220:249–269, 2006.
[20] K. Mattsson, M. Svärd, M. H. Carpenter, and J. Nordström. High-order accurate computations for unsteady aerodynamics. Computers & Fluids, 36:636–649, 2006.
[21] K. Mattsson, M. Svärd, and J. Nordström. Stable and Accurate Artificial Dissipation. J. Sci. Comput., 21(1):57–79, August 2004.
[22] K. Mattsson, M. Svärd, and M. Shoeybi. Stable and accurate schemes for the compressible navier-stokes equations. J. Comput. Phys., 227(4):2293–2316, 2008.
[23] M. Motamed, M. C. Babiuc, B. Szilagyi, H.-O. Kreiss, and J. W Winicour. Finite difference schemes for second order systems describing black holes. Physical Review D, 73:124008, 2006.
[24] J. Nordström and M. H. Carpenter. Boundary and interface conditions for high-order finite-difference methods applied to the Euler and Navier-Stokes equations. J. Comput. Phys., 148:341–365, 1999.
[25] J. Nordström and M. H. Carpenter. High-order finite difference methods, multidimensional linear problems, and curvilinear coordinates. J. Comput. Phys., 173:149–174, 2001.
[26] J. Nordström and J. Gong. A stable hybrid method for hyperbolic problems. J. Comput. Phys., 212:436–453, 2006.
[27] J. Nordström, K. Mattsson, and R. C. Swanson. Boundary conditions for a divergence free velocity-pressure formulation of the incompressible navier-stokes equations. J. Comput. Phys., 225:874–890, 2007.
[28] P. Olsson. Summation by parts, projections, and stability I. Math. Comp., 64:1035, 1995.
[29] P. Olsson. Summation by parts, projections, and stability II. Math. Comp., 64:1473, 1995.
[30] F. Pretorius. Simulation of binary black hole spacetimes with a harmonic evolution scheme. Classical and Quantum Gravity, 23(16):S529–S552, 2006.
[31] S. De Rango and D. W. Zingg. High-order aerodynamic computations on multi block grids. AIAA Paper, 2001-2631, 2001.
[32] B. Sjogreen. High order centered difference methods for the compressible Navier-Stokes equations. Technical report 01.01, RIACS, NASA Ames Research Center, 2001.

[33] J. C. Strikwerda. High-order-accurate schemes for incompressible viscous flow. Int. J. Numer. Method. Fluids, 24:715–734, 1997.
[34] M. Svärd, M. H. Carpenter, and J. Nordström. A stable high-order finite difference scheme for the compressible Navier-Stokes equations, far-field boundary conditions. J. Comput. Phys., 225:1020–1038, February 2008.
[35] M. Svärd, M. H. Carpenter, and J. Nordström. A stable high-order finite difference scheme for the compressible Navier-Stokes equations, no-slip wall boundary conditions. J. Comput. Phys., 227:4805–4824, May 2008.
[36] M. Svärd and J. Nordström. On the order of accuracy for difference approximations of initial-boundary value problems. J. Comput. Phys., 218:333–352, October 2006.
[37] B. Szilagyl, H.-O. Kreiss, and J. W Winicour. Modeling the black hole excision problem. Phys. Rev. D, 71:104035, 2005.
[38] D. W. Zingg, S. De Rango, M. Nemec, and T. H. Pulliam. Comparison of several spatial discretizations for the Navier-Stokes equations. AIAA Paper, 99-3260, 1999.